The Transformation of Salinity Variance: A New Approach to Quantifying the Influence of Straining and Mixing on Estuarine Stratification

XIANGYU LI

State Key Laboratory of Estuarine and Coastal Research, East China Normal University, Shanghai, China, and Woods Hole Oceanographic Institution, Woods Hole, Massachusetts

W. ROCKWELL GEYER

Woods Hole Oceanographic Institution, Woods Hole, Massachusetts

JIANRONG ZHU AND HUI WU

State Key Laboratory of Estuarine and Coastal Research, East China Normal University, Shanghai, China

(Manuscript received 20 September 2017, in final form 13 January 2018)

ABSTRACT

The roles of straining and dissipation in controlling stratification are derived analytically using a vertical salinity variance method. Stratification is produced by converting horizontal variance to vertical variance via straining, that is, differential advection of horizontal salinity gradients, and stratification is destroyed by the dissipation of vertical variance through turbulent mixing. A numerical model is applied to the Changjiang estuary in order to demonstrate the salinity variance balance and how it reveals the factors controlling stratification. The variance analysis reveals that dissipation reaches its maximum during spring tide in the Changjiang estuary, leading to the lowest stratification. Stratification increases from spring tide to neap tide because of the increasing excess of straining over dissipation. Throughout the spring–neap tidal cycle, straining is almost always larger than dissipation, indicating a net excess of production of vertical variance relative to dissipation. This excess is balanced on average by advection, which exports vertical variance out of the estuarine region into the plume. During neap tide, tidal straining shows a general tendency of destratification during the flood tide and restratification during ebb, consistent with the one-dimensional theory of tidal straining. During spring tide, however, positive straining occurs during flood because of the strong baroclinicity induced by the intensified horizontal salinity gradient. These results indicate that the salinity variance method provides a valuable approach for examining the spatial and temporal variability of stratification in estuaries and coastal environments.

1. Introduction

With the freshwater input from the river and saltwater input from the ocean, an estuary produces intermediate salinity water and exports the brackish water back into the ocean. This mixing process fundamentally depends on the horizontal salinity gradient between the riverine freshwater and the oceanic saltwater, which is a fundamental characteristic of estuaries (Nunes Vaz et al. 1989). This horizontal salinity gradient drives estuarine circulation, which provides the mean shear that strains the horizontal salinity gradient, giving rise to stratification (Hansen and Rattray 1966). Vertical stratification is another essential estuarine variable, and it has significant influence on various estuarine processes by affecting vertical mixing (Bowden 1981; Geyer 1993). Stratification is governed by the competition between straining caused by the interaction of the horizontal salinity gradient and vertical shear and turbulent mixing caused by tides (Simpson et al. 1990). Thus, understanding the variability of estuarine stratification depends fundamentally on the balance between straining and mixing.

The time-mean stratification varies in different estuaries, leading to the familiar classification of estuaries according to the intensity of stratification: salt wedge, strongly stratified, partially mixed, and well mixed (Cameron and Pritchard 1963). This classification neglects the pronounced time variability of stratification,

Corresponding author: Xiangyu Li, xlisklec@gmail.com

DOI: 10.1175/JPO-D-17-0189.1

most notably spring–neap and flood–ebb variation (Haas 1977; Nepf and Geyer 1996; Peters 1997). Stratification has particular dynamical significance because of its influence on turbulence. The variation of stratification may result in a 100-fold variation in the intensity of vertical mixing in an estuary (e.g., Peters and Bokhorst 2000). The variation in stratification in turn affects the strength of the vertical shear, thus affecting the intensity of straining, which provides the source for stratification. Thus, the interaction between stratification, mixing, and shear represents a strongly coupled, nonlinear system that exhibits abrupt transitions between stratified and well-mixed conditions associated with the spring–neap cycle (Haas 1977; Nunes Vaz et al. 1989; Bowen and Geyer 2003).

Marked variations in stratification may also occur within the tidal cycle, as first described by Simpson et al. (1990) in context with the tidal straining of the horizontal salinity gradient. These tidal variations in stratification may in turn provide a driving force for the mean estuarine circulation via nonlinear interaction between the tidal shear and the mixing (Jay and Smith 1990). Spatial variations in stratification may be as important as temporal, particularly in regions of rapid variation in depth or estuarine cross-sectional area (Geyer and Ralston 2015). However, the influence of spatial gradients of stratification on the overall balance of stratification in estuaries has received much less attention than the temporal variability.

Burchard and Rennau (2008) introduced the salinity variance equation as a means of linking stratification, straining, and mixing in estuaries, with a particular application to the Baltic Sea. The work of Burchard and Rennau is related to a paper by Stern (1968), who used the salinity variance equation to demonstrate that the global integral of mixing of salt in the ocean can be related to boundary fluxes of freshwater via evaporation, precipitation, and runoff. Stern's approach has more conceptual than practical utility because of the difficulty of quantifying variations of boundary fluxes at global scales, but it may find application in estuaries caused by the strong and relatively well-constrained boundary inputs of fresh and saltwater.

The variance approach is particularly amenable to treatment in numerical models where all of the terms in the variance equation can be quantified. The validity of this analysis with respect to actual estuaries depends on the skill of the model at reproducing observed variability of stratification, which sensitively depends on the model parameterization of turbulent mixing. Turbulence closure in oceanographic models has advanced to the point at which mixing in estuaries can be reproduced with adequate skill to reproduce detailed variability of stratification (e.g., Warner et al. 2005). However, Burchard and Rennau (2008) have demonstrated, using the salinity variance method, that substantial mixing may be the result of numerical discretization errors. While these numerical errors are not negligible, the fidelity of the model in predicting variations in stratification requires that the combined contributions of resolved (via the turbulence closure) and numerical mixing are consistent with the total "true" mixing in the field setting. The use of the salinity variance method allows the contributions of resolved and numerical mixing to be compared and thus to assess whether numerical mixing seriously compromises the representation of the dynamics of stratification. The insights gained from the analysis of variance in numerical models will provide guidance in the application of the method to field studies, notably for the quantification of straining and vertical mixing as they influence stratification.

In this paper, we use the salinity variance equation to quantify the net influence of straining and mixing on variation of estuarine stratification, with application to the tidal and spring–neap variability of the Changjiang estuary. In section 2, we describe the analytical method of the salinity variance equation. Section 3 presents the detailed description of spatial and temporal patterns of the stratification, straining, and mixing in the Changjiang estuary based on numerical model results. The flood–ebb asymmetry in tidal straining, the relationship between dissipation of variance and buoyancy flux, and the relationship between Simpson number Si and stratification are discussed in section 4. And finally, section 5 gives the conclusions.

2. Theory

Considering a three-dimensional domain, for example, an entire estuary, we can decompose the salinity as $S = \langle S \rangle + S'_{\text{tot}}$, where angle brackets denote the volume average, and a prime with subscript tot denotes the deviation from the total average. We start from the Reynolds-averaged salt conservation advection–diffusion equation:

$$\frac{\partial S}{\partial t} + \mathbf{u} \cdot \nabla S - \nabla \cdot (\mathbf{K} \nabla S) = 0, \tag{1}$$

where $\mathbf{u}$ is the three-dimensional velocity vector, and $\mathbf{K}$ is the diffusivity tensor. Consistent with most oceanographic modeling applications, only the diagonal elements of the tensor are considered: K_{xx}, K_{yy}, and K_{zz} being eddy diffusivity coefficients in three dimensions and other off-diagonal elements in $\mathbf{K}$ being 0. In this way, we obtain the matrix product $\mathbf{K}\nabla S = (K_{xx}\,\partial S/\partial x,\ K_{yy}\,\partial S/\partial y,\ K_{zz}\,\partial S/\partial z)$ to be the vector of three-dimensional diffusive salt fluxes.

By applying the decompositions $S = \langle S \rangle + S'_{\text{tot}}$ and $\mathbf{u} = \langle \mathbf{u} \rangle + \mathbf{u}'$ ($\mathbf{u}'$ indicates the velocity relative to the body

of water in the entire domain), a conservation equation for the mean salinity may be derived:

$$\frac{\partial\langle S\rangle}{\partial t}+\langle\mathbf{u}\rangle\cdot\nabla\langle S\rangle+\langle\mathbf{u}'\cdot\nabla S'_{\text{tot}}\rangle-\nabla\cdot(\mathbf{K}\nabla\langle S\rangle)=0. \tag{2}$$

Taking the difference between Eqs. (1) and (2) results in

$$\frac{\partial S'_{\text{tot}}}{\partial t}+\langle\mathbf{u}\rangle\cdot\nabla S'_{\text{tot}}+\mathbf{u}'\cdot\nabla\langle S\rangle+\mathbf{u}'\cdot\nabla S'_{\text{tot}}-\langle\mathbf{u}'\cdot\nabla S'_{\text{tot}}\rangle-\nabla\cdot(\mathbf{K}\nabla S'_{\text{tot}})=0. \tag{3}$$

Multiplying Eq. (3) by $2S'_{\text{tot}}$, we arrive at the salinity variance equation:

$$\frac{\partial(S'_{\text{tot}})^2}{\partial t}+\langle\mathbf{u}\rangle\cdot\nabla(S'_{\text{tot}})^2+2\mathbf{u}'S'_{\text{tot}}\cdot\nabla\langle S\rangle+\mathbf{u}'\cdot\nabla(S'_{\text{tot}})^2-2S'_{\text{tot}}\langle\mathbf{u}'\cdot\nabla S'_{\text{tot}}\rangle-[2\nabla\cdot(S'_{\text{tot}}\mathbf{K}\nabla S'_{\text{tot}})-2(\mathbf{K}\nabla S'_{\text{tot}})\cdot(\nabla S'_{\text{tot}})]=0. \tag{4}$$

Note that $2S'_{\text{tot}}\nabla\cdot(\mathbf{K}\nabla S'_{\text{tot}})$ has been rewritten via product rule. Since $\langle S\rangle$ is constant in space, $\nabla\langle S\rangle=0$, a dynamic equation for the salinity variance $(S'_{\text{tot}})^2$ may be derived:

$$\frac{\partial(S'_{\text{tot}})^2}{\partial t}+\nabla\cdot[\mathbf{u}(S'_{\text{tot}})^2-\mathbf{K}\nabla(S'_{\text{tot}})^2]-2S'_{\text{tot}}\langle\mathbf{u}'\cdot\nabla S'_{\text{tot}}\rangle=-2(\mathbf{K}\nabla S'_{\text{tot}})\cdot(\nabla S'_{\text{tot}}). \tag{5}$$

Next, we make some scaling estimates that indicate that some of the terms are negligible. First, the divergences of horizontal diffusive fluxes $\partial[K_{xx}\,\partial(S'_{\text{tot}})^2/\partial x]/\partial x$ and $\partial[K_{yy}\,\partial(S'_{\text{tot}})^2/\partial y]/\partial y$ are much smaller than vertical because of the large horizontal scales compared to vertical scales in estuaries, so these terms are neglected. Also, the horizontal components of mixing term $-2K_{xx}(\partial S'_{\text{tot}}/\partial x)^2$ and $-2K_{yy}(\partial S'_{\text{tot}}/\partial y)^2$ are relatively small compared to vertical mixing $-2K_{zz}(\partial S'_{\text{tot}}/\partial z)^2$, again based on the typical aspect ratio of the estuarine regime.

The vertical integral of the divergence of vertical diffusive flux $\partial[K_{zz}\,\partial(S'_{\text{tot}})^2/\partial z]/\partial z$ is zero based on the constraint that the vertical turbulent flux $K_{zz}\,\partial(S'_{\text{tot}})^2/\partial z$ vanishes at the surface and bottom. Also, when (5) is integrated over the volume V, $\langle S'_{\text{tot}}\rangle$ is zero, so the integral of $-2S'_{\text{tot}}\langle\mathbf{u}'\cdot\nabla S'_{\text{tot}}\rangle$ is also zero, thus yielding

$$\frac{\partial\iiint(S'_{\text{tot}})^2\,dx\,dy\,dz}{\partial t}+\oint_B\int\mathbf{u}(S'_{\text{tot}})^2\,dz\cdot\mathbf{n}\,dl=-\iiint 2K_{zz}\left(\frac{\partial S}{\partial z}\right)^2dx\,dy\,dz, \tag{6}$$

where $\oint_B dl$ denotes the line integral over the boundary of the domain, with $\mathbf{n}$ being the outward-pointing unit normal field of the boundary.

Equation (6) indicates that the rate of change of salinity variance inside a domain is controlled by only two quantities: the net flux of salinity variance into the domain and the dissipation of variance caused by mixing inside the domain.

Equation (6) demonstrates that the only source of variance to the domain comes from the boundary transport. In an estuary, the input of variance comes only from the freshwater at the river boundary and the saltwater at the ocean boundary. We follow the suggestion of Burchard and Rennau (2008) and Burchard et al. (2009) to refer to the term on the right side of Eq. (6) as "mixing," since it represents the action of homogenizing salinity by dissipating salinity variance. This term is always negative (with the presence of salinity gradient), indicating that mixing always diminishes salinity variance.

Equation (6) represents the total variance, which is made up of both vertical variance caused by stratification and horizontal variance caused by horizontal salinity gradients. The conversion between horizontal and vertical variance comes about because of straining—the action of vertical shears on horizontal salinity gradients. Next, let us introduce the definitions of vertical variance and horizontal variance.

Considering a single vertical water column instead of the entire three-dimensional domain, we may decompose the salinity as $S=\overline{S}+S'_v$, where an overbar denotes the vertical average, and a prime with subscript v denotes deviation from the vertical average. With this definition, $(S'_v)^2$ can be used to represent the vertical salinity variance. Consequently, let $S'_h=S'_{\text{tot}}-S'_v$, denote the subtraction of vertical deviation from the total deviation, and then $(S'_h)^2$ can be used to represent the horizontal salinity variance. Note that S'_h has no vertical variation (since $S'_h=\overline{S'_{\text{tot}}}=\overline{S'_h}$), so $\int S'_h\cdot S'_v\,dz=S'_h\int S'_v\,dz=0$. Therefore, we can prove that the vertical integral of total variance is made up of both the integral of horizontal variance and integral of vertical variance:

$$\int(S'_{\text{tot}})^2\,dz=\int(S'_h)^2\,dz+\int(S'_v)^2\,dz, \tag{7}$$

and consequently

$$\underbrace{\iiint(S'_{\text{tot}})^2dx\,dy\,dz}_{\text{Total Variance}}=\underbrace{\iiint(S'_h)^2dx\,dy\,dz}_{\text{Horizontal Variance}}+\underbrace{\iiint(S'_v)^2\,dx\,dy\,dz}_{\text{Vertical Variance}}. \tag{8}$$

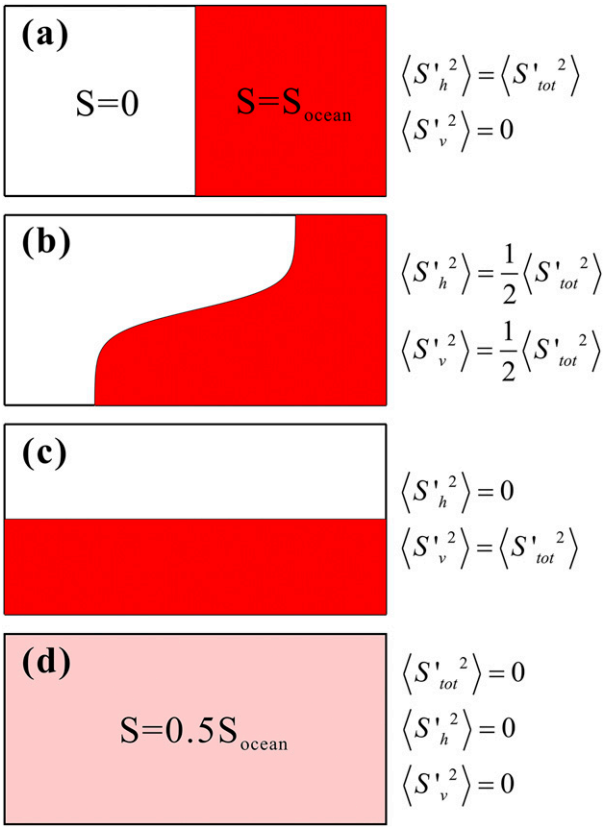

FIG. 1. Schematic of a lock-exchange experiment: (a) the initial state with freshwater on the left side and saltwater on the right side, (b) a transient state at the point at which the volume-averaged vertical salinity variance equals the horizontal variance, (c) the final state if there is no mixing, and (d) the ultimate state with the presence of mixing.

Lock exchange is the simplest case for illustrating the conversion of horizontal to vertical variance via straining (Fig. 1). Consider an initial state with freshwater on one side of a tank and saltwater on another side (Fig. 1a). In this initial configuration all of the variance is in the horizontal dimension. As lock exchange develops because of the horizontal density gradient: the horizontal variance decreases and vertical variance increases (Fig. 1b). In an idealized case with no mixing, the total variance remains constant. The final state of this idealized case (assuming no mixing but including energy dissipation to eliminate transient seiches), all of the variance is confined to the vertical (Fig. 1c). Alternatively, if mixing is included, eventually all of the salinity variance is consumed (Fig. 1d), given no boundary fluxes of variance.

We now explore the conservation of vertical salinity variance $(S'_v)^2$. We may also start from the Reynolds-averaged salt conservation advection–diffusion equation [Eq. (1)], follow similar steps as Eqs. (2) ~ (3), and we arrive at

$$\frac{\partial (S'_v)^2}{\partial t} + \bar{\mathbf{u}} \cdot \nabla (S'_v)^2 + 2\mathbf{u}'_v S'_v \cdot \nabla \bar{S} + \mathbf{u}'_v \cdot \nabla (S'_v)^2 - 2S'_v \overline{\mathbf{u}'_v \cdot \nabla S'_v} - [2\nabla \cdot (S'_v \mathbf{K} \nabla S'_v) - 2(\mathbf{K}\nabla S'_v) \cdot (\nabla S'_v)] = 0, \tag{9}$$

where $\mathbf{u} = \bar{\mathbf{u}} + \mathbf{u}'_v$.

After rearranging, the dynamic equation for the vertical salinity variance $(S'_v)^2$ may be formulated as

$$\frac{\partial (S'_v)^2}{\partial t} + \nabla \cdot [\mathbf{u}(S'_v)^2 - \mathbf{K}\nabla (S'_v)^2] - 2S'_v \overline{\mathbf{u}'_v \cdot \nabla S'_v} = -2\mathbf{u}'_v S'_v \cdot \nabla \bar{S} - 2(\mathbf{K}\nabla S'_v) \cdot S'_v, \tag{10}$$

which resembles Eq. (5) in Burchard and Rennau (2008). The difference between Eq. (10) in this paper and Eq. (5) in Burchard and Rennau's paper is that we average spatially, whereas they average temporally.

We also neglect divergences of horizontal diffusive fluxes and horizontal components of the mixing term, as we did for Eq. (6), based on the same argument that horizontal scales are much larger than vertical. When Eq. (10) is vertically integrated, the integral of term $2S'_v \overline{\mathbf{u}'_v \cdot \nabla S'_v}$ vanishes, thus resulting in

$$\underbrace{\frac{\partial \int (S'_v)^2 \, dz}{\partial t}}_{\text{Tendency}} + \nabla_h \cdot \underbrace{\int \mathbf{u}_h (S'_v)^2 \, dz}_{\text{Advection}} = \underbrace{\int -2\mathbf{u}'_v S'_v \cdot \nabla \bar{S} \, dz}_{\text{Straining}} - \underbrace{\int 2K_{zz} \left(\frac{\partial S}{\partial z}\right)^2 dz}_{\text{Dissipation (or Mixing)}}, \tag{11}$$

where ∇_h denotes the horizontal gradient operator, and $\mathbf{u}_h$ denotes the horizontal velocity vector.

Unlike Eq. (6), Eq. (11) has an internal source term, the straining term $-2\mathbf{u}'_v S'_v \cdot \nabla \bar{S}$, which describes the local conversion of horizontal variance to vertical variance. This conversion is conducted by the straining of the horizontal salinity gradient by differential advection in the vertical, which was elegantly demonstrated by Simpson et al. (1990).

The area integral of the dissipation term in Eq. (11) is identical to the RHS of (6), indicating that for the environments in which the horizontal scales are much larger than the vertical, the elimination of total variance is essentially performed by destroying vertical variance. Therefore, the mixing of salinity in an estuary is essentially a three-step process: first, salinity variance enters the estuary by means of freshwater from the river and saltwater from the ocean; second, straining converts horizontal variance into vertical variance by tilting the isohalines; and finally, turbulent mixing destroys salinity variance by its action on vertical variance.

Now we explore the properties of horizontal salinity variance. Horizontal variance is associated with horizontal salinity gradient, since $S'_h = \overline{S} - \langle S \rangle$ and consequently $\nabla(S'_h) = \nabla\overline{S}$. Thus, the straining term in the vertical variance equation (11) requires the presence of horizontal variance.

By subtracting Eq. (10) from Eq. (5), and then making the volume integral, one may obtain the dynamic equation for the horizontal salinity variance $(S'_h)^2$:

$$\frac{\partial \iiint (S'_h)^2 dx\,dy\,dz}{\partial t} + \oint_B \int \overline{\mathbf{u}}(S'_h)^2 dz \cdot \mathbf{n}\, dl + \oint_B \int 2\mathbf{u}'_v S'_v dz \cdot S'_h \mathbf{n}\, dl = \iiint 2\mathbf{u}'_v S'_v \cdot \nabla\overline{S}\, dx\,dy\,dz. \quad (12)$$

Equation (12) indicates that horizontal variance is influenced by the boundary advection, the boundary straining caused by sheared flow, and the local straining, with the last term occurring with the opposite sign in the vertical variance equation [Eq. (11)], demonstrating that the straining term represents the exchange between horizontal and vertical variance. The straining term may be of either sign, as illustrated by the process of tidal straining (Simpson et al. 1990), in which horizontal variance is converted to vertical during ebb and the reverse happens during flood tide. Because the destruction of variance only happens in the vertical variance equation, there must be a net flux of variance from horizontal to vertical, so the straining term must on average provide a transfer from horizontal to vertical variance. This is consistent with the classic formulation for the estuarine stratification balance (Hansen and Rattray 1965).

3. Stratification, straining, and mixing in the Changjiang estuary

a. The Changjiang estuary and the numerical model

The Changjiang estuary has a 90-km-wide river mouth (Fig. 2), discharging an average of 30 000 $m^3 s^{-1}$ of freshwater into the East China Sea. The maximum surface salinity anomaly occurs in summer when the averaged river discharge reaches 45 000 $m^3 s^{-1}$. The northeastward extension of Changjiang River plume can spread 450 km away from the river mouth (Moon et al. 2010). Similar to the Amazon, the Changjiang estuary is pushed out onto the shallow, inner shelf, making itself essentially an energetic, bottom-attached river plume (Geyer et al. 1996; Yankovsky and Chapman 1997). Saltwater intrusion usually happens in winter when the averaged river discharge drops to 11 000 $m^3 s^{-1}$, with the salt intrusion enhanced by landward Ekman transport induced by northerly winds (Wu and Zhu 2010; Li et al. 2014).

The numerical model used in this study was developed and validated by Wu and Zhu (2010) and Qiu and Zhu (2013). This model uses the Mellor–Yamada 2.5 turbulence closure (Mellor and Yamada 1982) with stability constants from Galperin et al. (1988) and wall function from Burchard (2001) to describe vertical mixing. Validation of the model using observed current and salinity data shows reasonable accuracy (Wu and Zhu 2010; Qiu and Zhu 2013; Li et al. 2014). Wind, waves, temperature variations, and suspended sediment were not included in order to focus on the variation of salinity variance controlled by the continuous freshwater input from the river and periodic saltwater input from the ocean controlled by tides.

b. The vertical salinity variance as a measure for stratification

The vertical salinity variance has not been traditionally used as a measure of stratification. Most commonly, stratification is quantified simply by the top-to-bottom salinity difference ΔS (Hansen and Rattray 1966; Haas 1977; Sutherland et al. 2011). Another measure of stratification with more relevance to the energetics is the potential energy anomaly

$$\phi = \rho_0 \beta g / h \int (\overline{S} - S) z\, dz \quad (13)$$

used by Simpson et al. (1990) to explore the energetics of estuarine mixing and often used a measure of stratification, where ρ_0 is a constant background density, $\beta \cong 7.7 \times 10^{-4}$ is the coefficient of saline expansion, g is the acceleration of gravity, and h is the water depth. However, neither ΔS nor ϕ has the simple conservation properties of the vertical salinity variance, so it would be useful to quantitatively link the vertical salinity variance to these more familiar and commonly used measures of stratification.

Figure 3 represents the relationship between the potential energy anomaly ϕ/h and vertical salinity variance $\overline{S'^2_v}$ (note that the inclusion of water depth is required for dimensional reasons) as well as the relationship between the top-to-bottom salinity difference ΔS and vertical salinity variance $\overline{S'^2_v}$ calculated with instantaneous salinity data of all the grid cells from the numerical model. The good correlations between ϕ/h and $\overline{S'^2_v}$ as well as between ΔS and $\overline{S'^2_v}$ provide confidence in using $\overline{S'^2_v}$ as a substitution for ϕ or ΔS for quantifying stratification. Constant factors $\sqrt{12}/(\rho_0 \beta g)$ and $1/\sqrt{12}$ are derived from the simple case of a linear salinity profile. For any vertically linear salinity profile

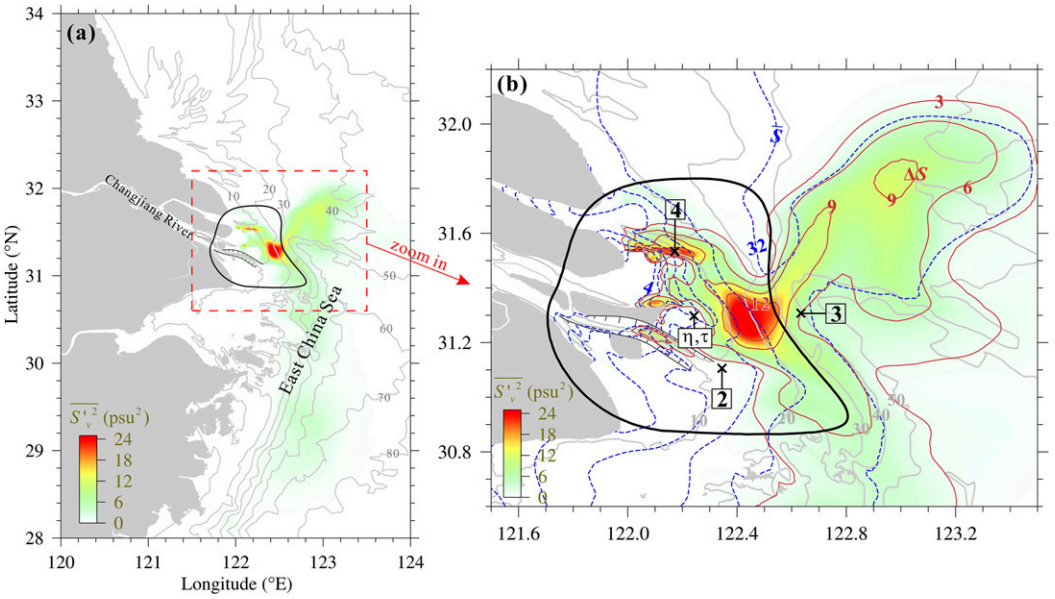

FIG. 2. (a) Map of the Changjiang estuary with the horizontal distribution of ebb-averaged $\overline{S_v'^2}$ during spring tide in color. (b) Zoom in of the area in the red dashed box in (a), with color still representing $\overline{S_v'^2}$ at the same scale. Red solid contours indicate the top-to-bottom salinity difference, with the interval of 3 psu. Blue dashed contours indicate the depth-averaged salinity, with the interval of 4 psu. In (a) and (b), the solid black circles represent the estuarine domain V used for calculations of volume-averaged quantities. In both panels, bathymetry is denoted in gray contours with an interval of 10 m. The seaward boundary of domain V roughly follows the 30-m isobath.

$$\sqrt{\overline{S_v'^2}} \equiv \left[\sqrt{12}/(\rho_0 \beta g)/h\right]\phi \equiv \left(1/\sqrt{12}\right)\Delta S. \qquad (14)$$

Other profile shapes that are representative of different parts of the Changjiang estuary (shown in Fig. 3) have different numerical constants but still show a linear relationship between the different measures of stratification.

Therefore, the vertical variance can readily be related to these other quantities, with only minor sensitivity to the shape of the vertical profile of salinity. Using the results of the simulation of the Changjiang estuary, the comparison of the salinity variance to these other stratification parameters shows consistent scaling that is readily explained theoretically using selected vertical salinity profiles.

The consistent relationship between $\overline{S_v'^2}$ and these other measures of stratification indicates that the salinity variance provides an equivalent means of quantifying stratification. This is also shown in Fig. 2 by the comparison of the spatial distribution of salinity variance to ΔS. The advantage of using salinity variance over these other quantities is to be able to exploit the simple form of the conservation of salinity variance so as to be able to quantify the factors responsible for its spatial and temporal variability. The distribution of salinity variance in Fig. 2 indicates that stratification reaches a maximum in distinct, localized zones of the estuarine outflow (red zones in Fig. 2b both have $\Delta S > 12$ psu). In the analysis that follows, we will use Eq. (11) to examine the processes responsible for the distribution of stratification and its variability through the spring–neap cycle.

c. *Spring–neap variation of salinity variance*

To examine the time-varying, spatially integrated variation of salinity variance, we take a circled region in the Changjiang estuary to define the control volume $V = \iiint dx\,dy\,dz$ (Fig. 2). This estuarine region starts at the river mouth where salinity is mostly 0 and ends at the 30-m isobath where salinity is around 32 psu. The outer limit of the control volume roughly follows the 30-m isobath. This volume was selected to encompass the most active regions of straining and mixing, effectively encompassing the estuarine zone but excluding the riverine zone and the far-field plume.

Each of the terms in Eq. (8) is estimated with the Changjiang model results to illustrate the spring–neap variations of the volume-averaged total salinity variance $\langle S_{\text{tot}}'^2 \rangle$, horizontal salinity variance $\langle S_h'^2 \rangle$, and vertical salinity variance $\langle S_v'^2 \rangle$ (Fig. 4). The spring–neap variability in tidal forcing is revealed both by the varying envelope of tidal elevation and the changes in the magnitude of

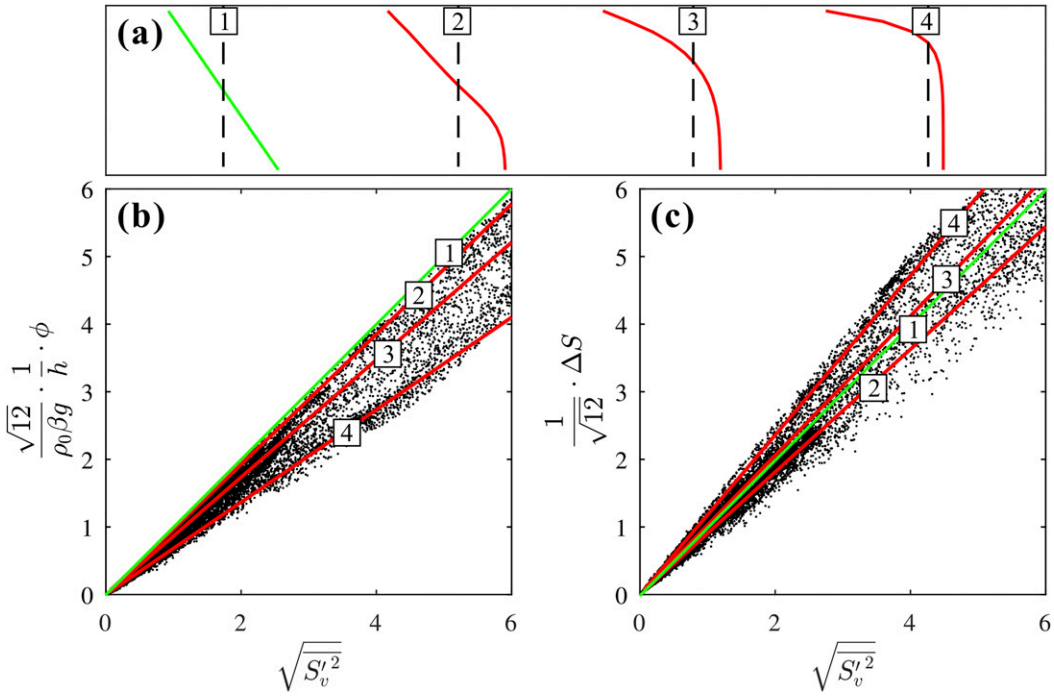

FIG. 3. (a) With the linear relations of four theoretical vertical profiles shown, comparisons between (b) ϕ and $\sqrt{S_v'^2}$ and (c) ΔS and $\sqrt{S_v'^2}$ of the instantaneous model data (dots) are represented. The green line 1 shows the relationship for a linear profile. The other three profiles correspond to representative profiles from the Changjiang estuary based on model results, the locations of which are signified by black crosses in Fig. 2.

the bottom stress, ranging from 0.2 Pa during neap tide to 0.8 Pa during spring tide (Fig. 4a). The spring–neap variability is mirrored in the vertical variance (Fig. 4b) with maxima occurring during the neaps and minima during springs, consistent with expectations of the spring–neap variation in estuarine stratification (Haas 1977). Total variance is dominated by horizontal variance, which is roughly constant. The spring–neap variability of the total variance is due mainly to the variations in vertical variance. Both total and horizontal variance show considerable tidal variability, mainly because of the advection across the boundaries of the control volume. It should be pointed out that the ratio between horizontal variance and vertical variance might be different in other estuaries, and it depends on the selection of the control volume, so the relative fraction of horizontal and vertical variance needs to be viewed in context with the specifications of that volume. For example, if the volume included only the river plume, a much larger fraction of the total variance would be made up of vertical variance. Because this particular control volume extends across the estuarine frontal zone, it receives a major fraction of its variance from the horizontal dimension. Note that the choice of the boundaries of the control volume affects the relative magnitudes of the horizontal and vertical variances. However, their variability should be less sensitive to the extent of the control volume as long as the estuarine gradient zone is fully resolved.

Interestingly, the horizontal variance shows little spring–neap variability, even though Eqs. (11) and (12) indicate that vertical variance is created at the expense of horizontal variance through the straining term. We surmise that the loss of horizontal variance to vertical is compensated by enhanced boundary fluxes of variance [Eq. (12)], although this issue was not explored further.

To examine the estuarine stratification balance, volume averages of all the terms in Eq. (11) are made, with the results shown in Fig. 5. Stratification (shaded in Fig. 5) increases while approaching neap tide, mainly because of the excess of straining over dissipation. Straining (red curve) varies through the spring–neap cycle, reaching its peak just before neap tides. Dissipation (blue) peaks during spring tides and drops during neaps because of variations in mixing intensity. Note that the dissipation as defined in Eq. (11) is positive definite, so it always acts to reduce salinity variance. Straining is almost always larger than dissipation,

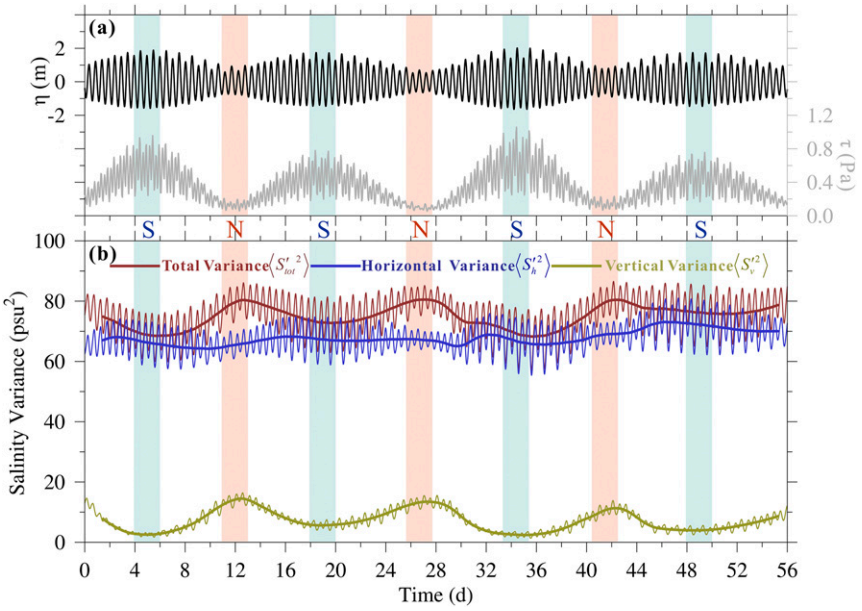

FIG. 4. (a) Time series of free surface elevation η (black line) and bottom stress τ (gray line) at one point in the domain V (location see black cross in Fig. 2). They also roughly represent the volume-averaged η and τ. (b) Time series of volume-averaged (domain location see Fig. 2) total variance, horizontal variance, and vertical variance in different colors. In (b), the 35-h low-pass filtered time series are also represented with thicker lines. Spring and neap tidal cycles are marked with capital letters S and N, respectively.

indicating a net excess of production of vertical variance relative to dissipation. This excess is balanced on average by advection, which exports vertical variance out of the estuarine region into the plume. The increase in straining between spring and neap tides and the decrease in dissipation leads to the marked increase in vertical salinity variance approaching neap tides. As the salinity variance increases, the export of variance increases, as indicated by the increased amplitude of advection (negative indicating export) during and just after the neap tide. The export of stratification drops to zero during and following spring tides. The unbalanced (residual) term is regarded as numerical mixing, which is further discussed in section 4b.

d. *Spatial pattern of stratification, straining, and mixing*

The spatial structure of the different terms contributing to the variations of stratification through the spring–neap cycle is shown in Fig. 6. The straining term has local maxima that correspond to the maxima in stratification (e.g., spot 1 in Fig. 6e). During spring tides, the maximum straining occurs in an elongated region in the northwestern part of the estuary (Fig. 6a). During neap tides this zone expands somewhat to the south, and another pronounced maximum occurs in the middle of the estuarine outflow (Fig. 6b). The broader spatial extent of strong straining during neap tides leads to larger integrated production of stratification than spring tides, as indicated in Fig. 5. A few zones of negative straining are evident, but positive straining greatly exceeds negative on average during both spring and neap tides.

Dissipation has a similar spatial distribution to straining (Figs. 6c,d), in large part because of the correspondence between high stratification and straining; note that dissipation depends quadratically on the vertical salinity gradient. While the spatial pattern of dissipation is similar to straining, its amplitude is not as high, leading to a net excess of production of stratification in the regions of maximum straining during both spring and neap tides (Figs. 6e,f). This excess is mainly balanced by advection, which carries vertical salinity variance along the outer edge of the estuarine zone and into the plume. At subtidal scales, the tendency term in Eq. (11) could be neglected compared to the other three terms, indicating that the net in Figs. 6e and 6f can be roughly regarded as the advection term. Therefore, a positive net indicates a region of divergence of stratification, and a negative net indicates convergence of stratification. Convergence of transport of vertical variance produces a local maximum of stratification offshore of the maximum straining zones (e.g., spot 2 in Fig. 6e).

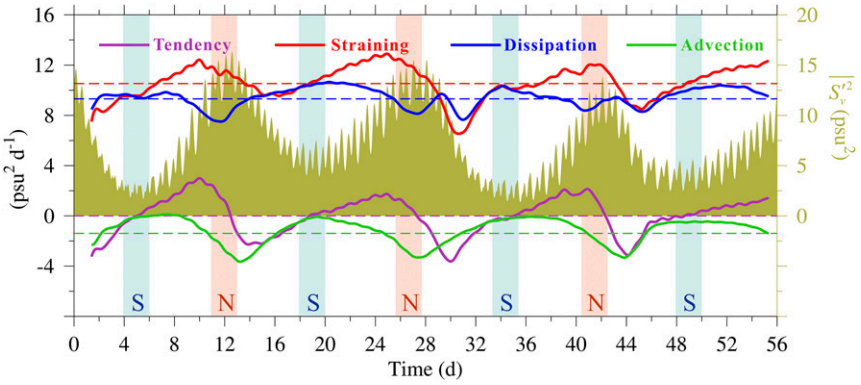

FIG. 5. Time series of terms in the vertical salinity variance equation are shown as solid lines in different colors, that is, tendency, straining, dissipation, and advection. All the terms are volume averaged as well as 35-h low-pass filtered. The dashed lines represent the time-averaged tendency, straining, dissipation, and advection terms over three spring–neap tidal cycles. The tidally varying vertical salinity variance is also shown as the olive green area. Spring and neap tidal cycles are marked with capital letters S and N, respectively.

Although advection of stratification plays an important role in redistributing the vertical variance in the estuary (Fig. 6), it is not as significant as straining or dissipation when volume averaged (Fig. 5), since the net flux of stratification across the boundary is relatively small. Nevertheless, the net export of stratification is the main source of stratification to the plume. Consistent with Wu et al. (2011, 2014), tidal rectification has a major influence on the trajectory of the plume in the absence of wind forcing. During spring tides, the plume is directed northeastward, while during neap tide, the plume turns southeast (Figs. 6e,f).

e. *The mechanism of straining at subtidal time scales*

At subtidal time scales, straining is almost always positive, during both spring tide and neap tide, as indicated in Figs. 6a and 6b and in more detail in Fig. 7. From Eq. (11), straining is the result of the vector product of $\mathbf{u}'_v S'_v$ and ΔS. Note that $\mathbf{u}'_v S'_v$ is the net salt flux driven by vertical variations in velocity and salinity, that is, the salt flux caused by the estuarine exchange flow (Lerczak et al. 2006). The direction of the estuarine salt flux is generally landward, balancing the net seaward salt flux caused by the river outflow. The strength of the straining depends on the strength of the exchange flow, the strength of the horizontal salinity gradient, and the angle between the salt flux and the salinity gradient.

The orientation and magnitude of the estuarine salt flux vectors are shown in Fig. 7. Note that the strongest salt fluxes tend to occur in regions of strong horizontal salinity gradient, and the salt flux has a significant component aligned with the salinity gradient. This combination of strong gradients and strong salt flux produces the zones of high straining observed during spring and neap tides. There are places where salt flux is large but straining is not correspondingly strong because the salt flux is parallel to the isohaline (e.g., site 3 and 5 in Fig. 7). There are also places where horizontal salinity gradients are strong but straining is weak because of the weak exchange flow (e.g., site 4 in Fig. 7). Therefore, the magnitudes of the estuarine salt flux and the subtidal horizontal salinity gradient as well as the orientation between these two vectors are equally important in maintaining strong tidally averaged straining.

Negative straining can also be observed where the direction of salt flux is ''countergradient,'' that is, toward high salinity (blue spots in Fig. 7). These regions are the result of destratification by tidal straining during the flood tide, so the tidally averaged conditions shown in Fig. 7 do not demonstrate the occurrence of the negative straining. The tidal variability of straining is discussed in more detail in section 4a.

4. Discussion

a. *Flood–ebb asymmetry in tidal straining*

To better understand the role of tidal straining versus tidally averaged straining in the Changjiang estuary, we indicate the spatial distribution of straining at different tidal conditions in Fig. 8. The straining that occurs during neap tide shows a general tendency of destratification during the flood tide (Fig. 8a), and restratification during ebb (Fig. 8b), consistent with the one-dimensional theory of tidal straining by Simpson et al. (1990). It should be pointed out that because of the complicated, three-dimensional distribution of the horizontal salinity field, positive straining can also be seen on flood during neap tide, and negative straining is present at some places on ebb during neap tide. But the

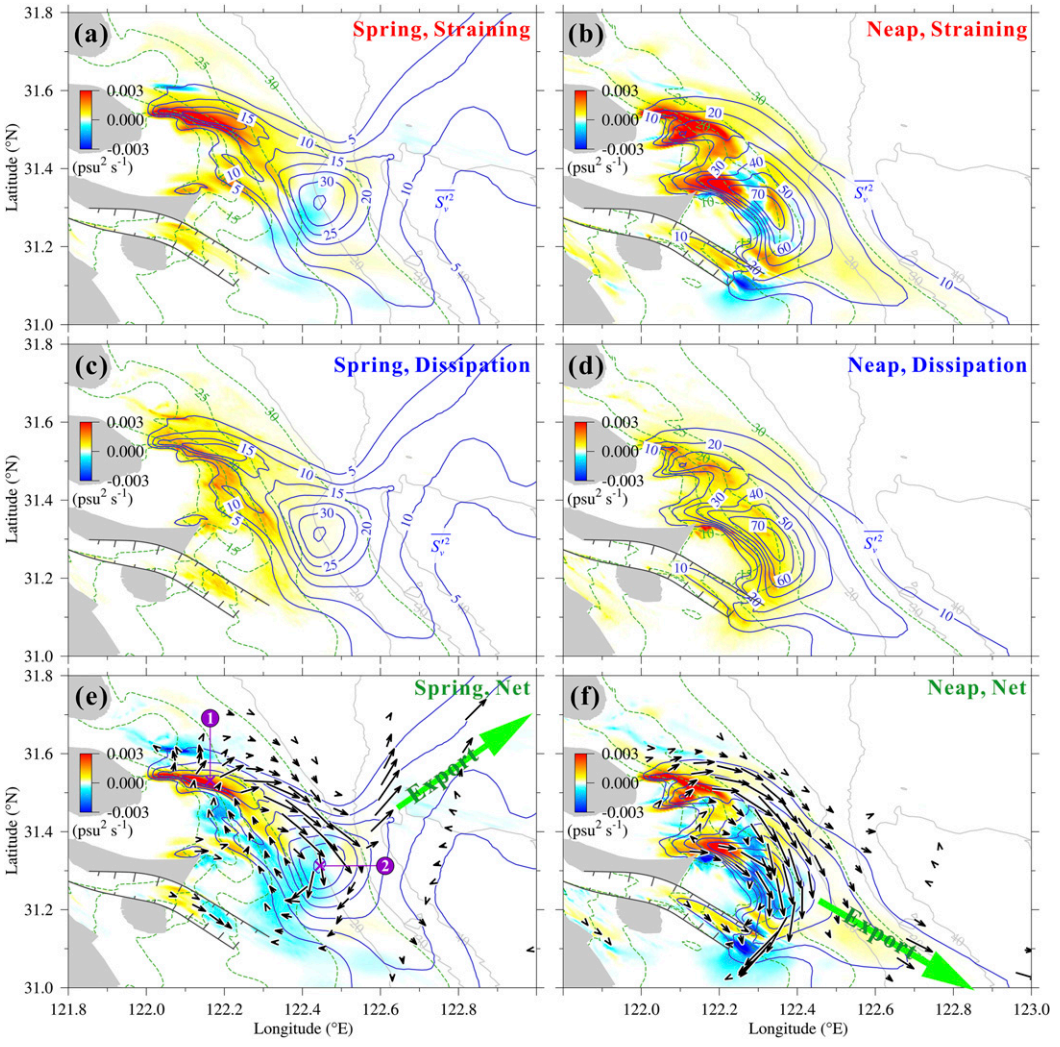

FIG. 6. Horizontal distribution (color) of the vertically averaged (top) straining, (middle) dissipation, and (bottom) net (straining − dissipation), with (left) spring average and (right) neap average. The blue contours denote the vertically averaged vertical variance $\overline{S_v'^2}$, with intervals of 5 psu^2 for spring tide and 10 psu^2 for neap tide. Two hot spots of stratification are signified by purple crosses in (e). Vertical-averaged salinities are represented in green dashed contours. Bathymetry shown by gray contours. Black arrows in (e) and (f) indicate the transport of vertical variance $h \cdot \overline{(uS_v'^2, vS_v'^2)}$, while the large green arrows signify directions of the export of stratification.

overall straining that occurs during neap tide is consistent with the conventional concept of tidal straining.

The spring tides show a different regime, however, in which positive straining occurs during both flood and ebb. To determine the mechanisms of straining during different tidal phases, a transect was specified roughly perpendicular to the isohalines shown as a purple dashed line on each of the panels of Fig. 8. Cross sections of velocity, horizontal salinity gradient, and straining are plotted on Fig. 9. An important difference between neaps and springs is salinity distribution. During neaps, the gradient region extends relatively uniformly along the section, whereas during spring tides a sharp front develops at the depth transition. This strong horizontal gradient results in a positive velocity shear in the upper water column during flood tide during the spring tide. This shear acts on the salinity gradient to produce positive straining, increasing the stratification. During neaps, the absence of strong baroclinic forcing allows the boundary-generated velocity shear to extend through the water column at this location, resulting in a destratifying tendency consistent with tidal straining.

Straining on ebb tide (Fig. 9, right-hand panels) is consistent with the tidal straining situation described by Simpson et al. (1990), in which the sense of the

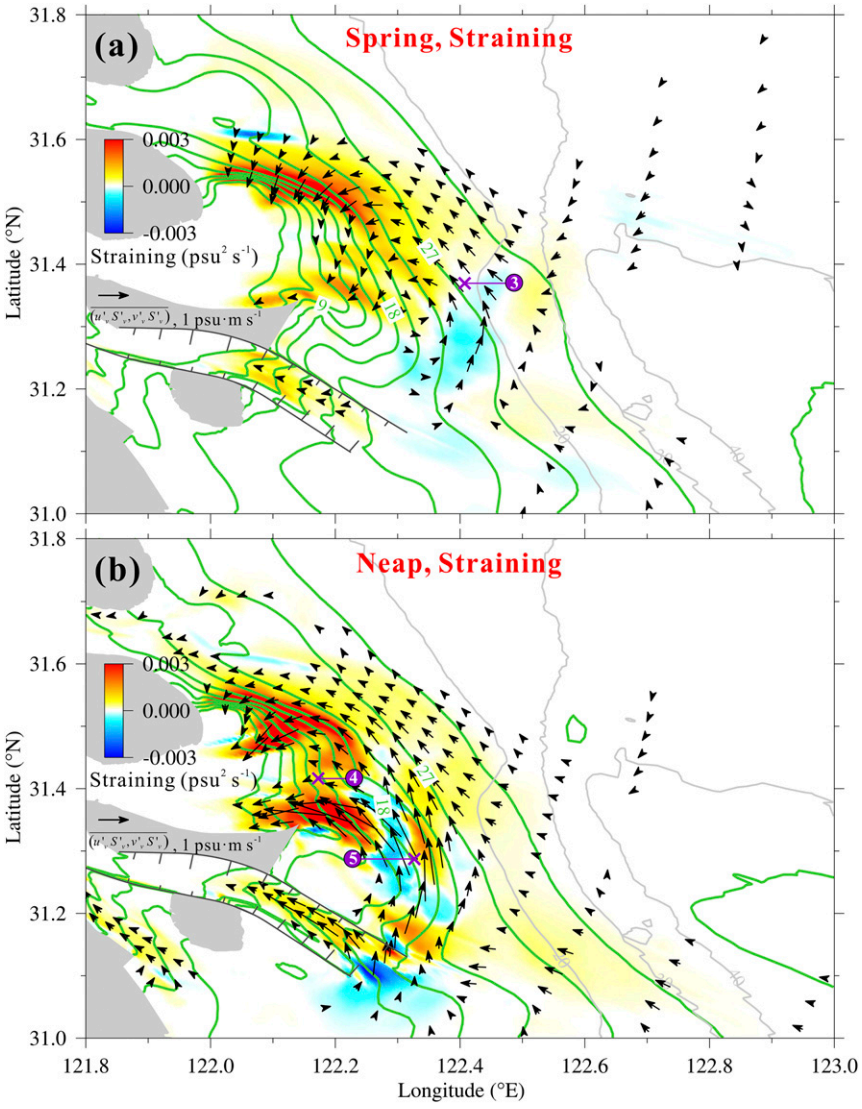

FIG. 7. Distributions of vertical-averaged straining (color), averaged during (a) spring tide and (b) neap tide. Depth-averaged salinities are represented in green contours, from 3 to 33 psu with the interval of 3 psu. Black arrows denote the vectors $(\overline{u'_v S'_v}, \overline{v'_v S'_v})$. Bathymetry is in gray contours.

boundary-generated shear reinforces the baroclinically generated shear, leading to strong positive straining. The strong shear tilts the isohalines by differential displacement and generates strong stratification (Figs. 9b,d). Note that it is the vertical deviation of velocity $\mathbf{u}'_v$ that performs the displacement, while the depth-averaged velocity $\overline{\mathbf{u}}$ advects the isohalines without converting horizontal variance to stratification.

This example indicates that with a strong enough salinity gradient, positive straining and persistent stratification can be maintained even during the strong mixing conditions of the spring tide. It remains to be explained why the gradient becomes so strong during spring tides.

During spring tide, a strong front develops during the late ebb tide (Figs. 10a,c). The strong bottom shear stress in the shallow water between 0 and 15 km allows the boundary-generated turbulence to extend throughout the water column, which reduces shear and stratification. Tidal advection carries the mixed water seaward. The salinity gradient greatly amplifies as the isohalines retreat because of the convergence at the depth transition at 17.5 km. This convergence leads to the formation of a "lift-off" front (Luketina and Imberger 1987) at the depth transition (Fig. 10c). The dynamics of the formation of a lift-off front have been described by various authors [e.g., Armi and Farmer 1986; Geyer and Ralston 2015; see review by Horner-Devine et al. (2015)], and the

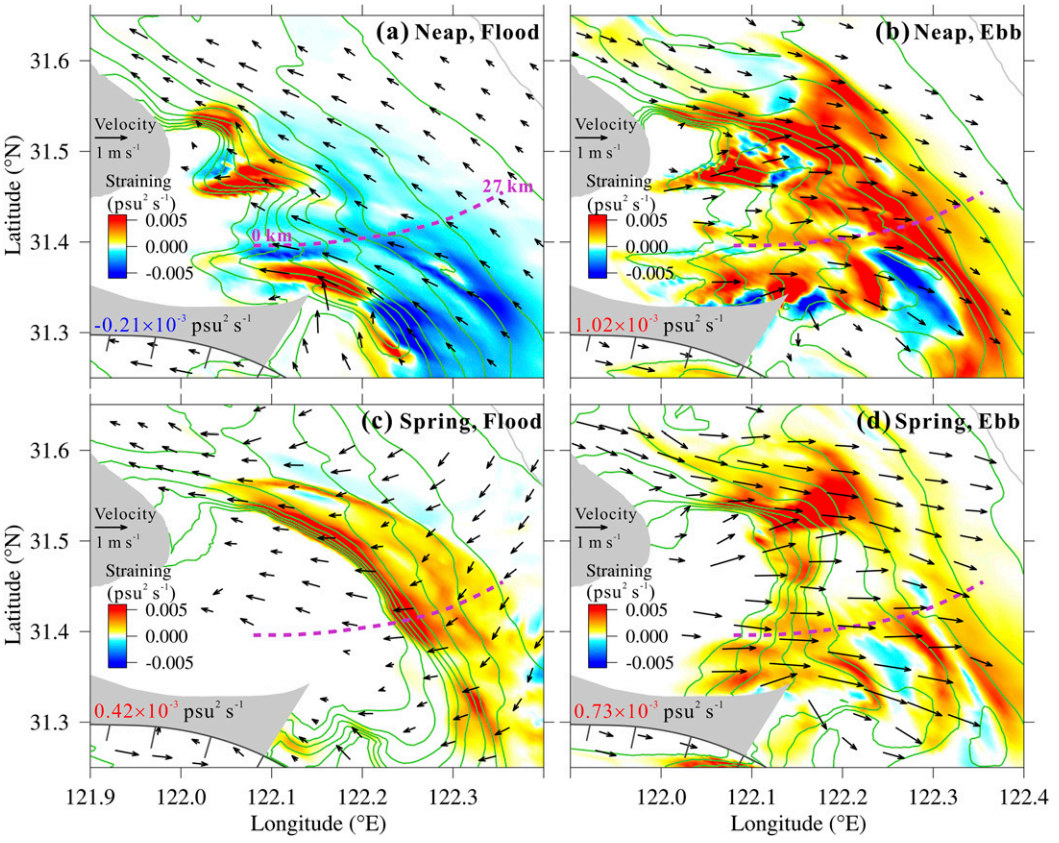

FIG. 8. Instantaneous distributions of vertical-averaged straining (color), taken on (a) flood tide and (b) ebb tide during spring tide as well as on (c) flood tide and (d) ebb tide during neap tide. Black arrows denote the depth-averaged velocities. Depth-averaged salinities are represented in green contours, from 3 to 33 psu with the interval of 3 psu. Spatial-averaged straining is shown in number for each panel. The position of transect SecN used in Figs. 9 and 10 is shown as a purple dashed line.

details will not be discussed here. The essence of the frontogenesis process is that supercritical conditions [with respect to the internal Froude number, as defined by Armi and Farmer (1986)] occur upstream of the depth transition, and critical conditions occur in the deeper water downstream. In this case the enhanced mixing during the ebb weakens the stratification on the shallow side, leading to supercritical conditions there that promote frontogenesis. In contrast, during the neap tide, the weaker mixing allows the maintenance of stratification over the shallow water, and the critical Froude number occurs landward of the depth transition (Fig. 10d), preventing the occurrence of frontogenesis.

b. *Relationship between dissipation of variance and buoyancy flux*

Dissipation of salinity variance $K_{zz}(\partial S/\partial z)^2$ can be expressed as the product of the buoyancy flux B and vertical salinity gradient $\partial S/\partial z$:

$$K_{zz}\left(\frac{\partial S}{\partial z}\right)^2 = \frac{B}{\beta g}\left(\frac{\partial S}{\partial z}\right). \tag{15}$$

The buoyancy flux is of central importance in the turbulent kinetic energy equation, as it represents the energy expended against gravity in mixing a stratified fluid (Tennekes and Lumley 1972). It is also linked to the production of turbulent kinetic energy $P = \tau\,\partial u/\partial z$ via the flux Richardson number $R_f = B/P$, where τ is shear stress. Therefore, it is instructive to compare the variability of B to the variability of salinity dissipation in the estuarine environment. Figure 11 shows the volume-averaged variation of these quantities in the Changjiang estuary simulations. Buoyancy flux B shows a strong spring–neap variation, consistent with the variation of turbulence production caused by variations in bottom stress (cf. Fig. 4). Dissipation also varies over the spring–neap cycle but with much smaller amplitude than the buoyancy flux. This is because $\partial S/\partial z$ is stronger during neap tide, compensating for much of the variability in buoyancy flux.

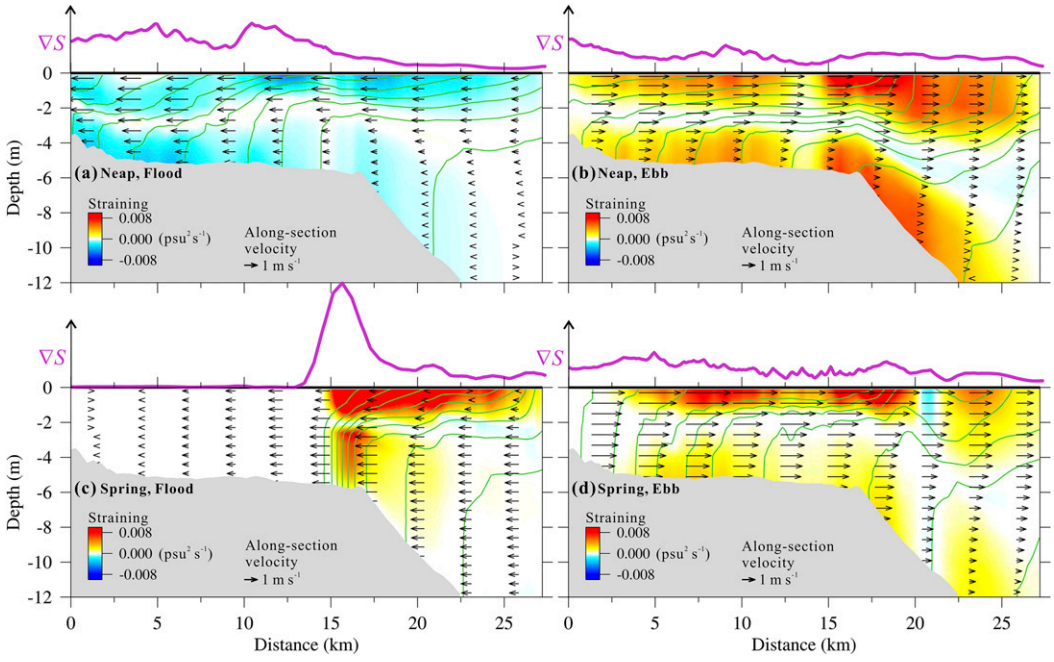

FIG. 9. Snapshots of straining (color) in the vertical at SecN taken at the same times as Fig. 8. Purple lines at the top of each panel indicate the strength of the horizontal salinity gradient. Black arrows show the along-section velocity. Green contours denote the salinity, with the interval of 3 psu. For the position of SecN, see Fig. 8.

Figure 11 also shows the contribution of numerical dissipation to the total dissipation. This is the mixing that results in the model because of discretization errors of the advection scheme that contribute to the total mixing shown in these model results. We did not include such discretization errors in our salinity variance calculations, but these errors did indirectly influence our estimates by decreasing vertical salinity gradients (Burchard et al. 2009), which could further lead to changes in both straining and mixing terms. However, the magnitude of numerical (unresolved) mixing is relatively small (~33%) compared to the total mixing in our results (Fig. 11). According to Rennau (2011), the numerically induced mixing may be of the same order of the physical mixing when modeling the advection of high density gradients.

c. *The Simpson number as a diagnostic for stratification*

The Simpson number

$$\mathrm{Si} = \beta g(\partial S/\partial x)h^2/(C_D U_T^2) \tag{16}$$

(Geyer and MacCready 2014) provides a measure of the straining by the horizontal salinity gradient and the destruction of stratification by mixing, where C_D is the drag coefficient and U_T is the amplitude of the depth-averaged tidal flow. It has been used to ascertain the balance between straining and mixing and also to determine whether or not an estuary is stratified (Simpson et al. 1990; Geyer and MacCready 2014). Burchard and Schuttelaars (2012) used different values of Si as a control parameter to characterize different scenarios from well-mixed estuarine flow to periodically stratified estuarine flow.

In the Changjiang simulations, Si variations roughly follow stratification (Fig. 12). During spring tides, the Simpson number falls below 1, corresponding to relatively weak stratification conditions. The sharp decrease in stratification between neaps and springs roughly corresponds to the point where Si drops below 1. However, the increase in stratification after spring tides commences well before Si increases to a value of 1. Thus, while Si provides a rough diagnostic of the balance between straining and mixing, other factors (such as mixing efficiency) also play a significant role in controlling the balance between straining and mixing.

5. Summary

This paper applies a vertical salinity variance methodology for studying the roles of straining and mixing in controlling stratification, applying the approach to the

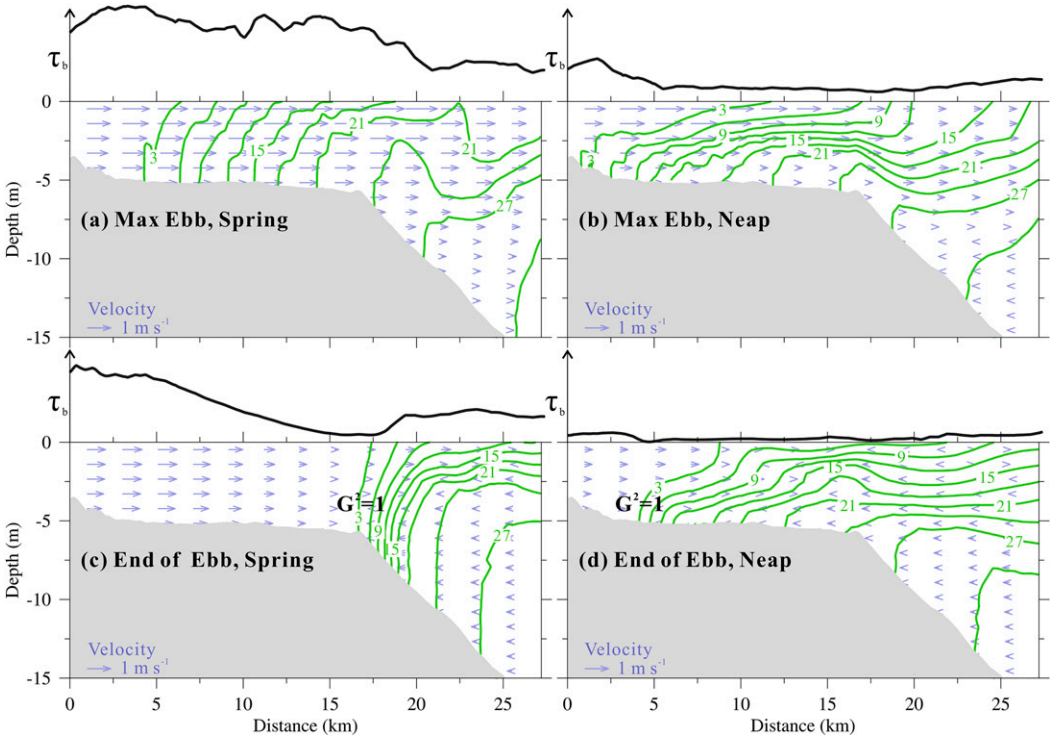

FIG. 10. Salinity distributions at SecN at (a),(b) max ebb and at (c),(d) end of ebb during (left) spring tide and (right) neap tide are represented by green contours. The black line at the top indicates the bottom shear stress. Along-section velocities are shown with light blue arrows; G is the composite Froude number as defined by Armi and Farmer (1986), calculated here by making layer approximations of the velocity and density distributions.

temporal and spatial variation of stratification in the Changjiang estuary. At the beginning, three kinds of salinity variances are introduced: the total variance, the horizontal variance, and the vertical variance, with the former being made up of the latter two. Then it is demonstrated that the vertical salinity variance can be used to quantify stratification. The vertical variance equation indicates that stratification is produced by the straining induced by the vertically differential advection of the horizontal salinity gradient, which represents the local conversion of horizontal variance to vertical variance. While straining provides exchange between horizontal and vertical variance, the dissipation of variance is accomplished only in the vertical dimension via the mixing of stratified fluid.

The Changjiang estuary has a strong spring–neap signal of stratification, providing an effective test case for applying the salinity variance approach to investigate straining and mixing. The spring–neap variations of stratification are the result of intensified straining during neap tides and intensified dissipation during spring tides. Throughout the spring–neap tidal cycle, straining is almost always larger than dissipation, indicating a net excess of production of vertical variance relative to dissipation. This excess is balanced on average by advection, which exports vertical variance out of the estuarine region into the plume. It is worth noting that, though advection is not as significant as straining or dissipation when volume averaged in the estuary, it plays an important role in the exchange of salinity variance between the ocean and the estuary: it brings total variance in the estuary and then brings vertical variance out. During both spring and neap tides, straining is intensified in localized regions of the strong horizontal salinity gradient. Two different mechanisms are observed in generating peak stratification regions in the Changjiang estuary. One is the great excess of straining over dissipation, which is balanced by the divergence of stratification. The other one is the convergence of the transport of stratification, which is balanced by dissipation and negative straining.

Tidally averaged straining is strongest where both the tidally averaged horizontal salinity gradient and the salt flux caused by the exchange flow are strongest. During neap tide, tidal straining shows a general tendency of destratification during the flood tide and restratification during ebb, consistent with the one-dimensional theory of tidal straining by Simpson et al. (1990). During spring tide, however, positive straining is found to occur during flood because of the strong baroclinicity induced by a

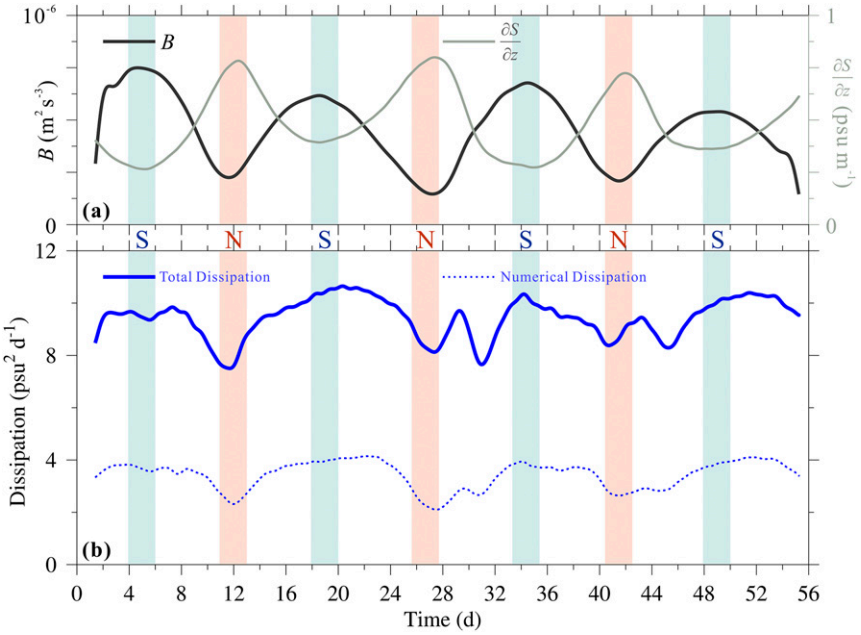

FIG. 11. (a) Buoyancy flux B (black line) and vertical salinity gradient $\partial S/\partial z$ (gray line). (b) The total dissipation (solid blue) and the numerical dissipation (dashed blue) are shown. All of these terms are averaged over estuarine domain V shown in Fig. 2 and 35-h low-pass filtered.

salinity front. This front results from the interaction of the strong tidal flow with abrupt bottom topography. This study shows that the straining process can be highly localized because of the presence of fronts; moreover, the localization of straining also results in local intensification of stratification and mixing. The Simpson number has been widely used to ascertain the balance between straining and mixing. In application to the Changjiang, Si provides a rough guide of the state of stratification of the system based on volume averages of the horizontal salinity gradient and bottom stress. A threshold value of Si $\sim$ 1 appears to distinguish between strongly stratified and weakly stratified regimes.

In conclusion, the salinity variance method provides a straightforward means of quantifying the mechanisms responsible for the creation and destruction of stratification in estuaries based on the application to the spatially and temporally complex Changjiang estuary. The method highlights the critical importance of regions of intensified salinity gradients in producing stratification. Not only do these regions show the most intense straining, they are also sites of the most intense mixing

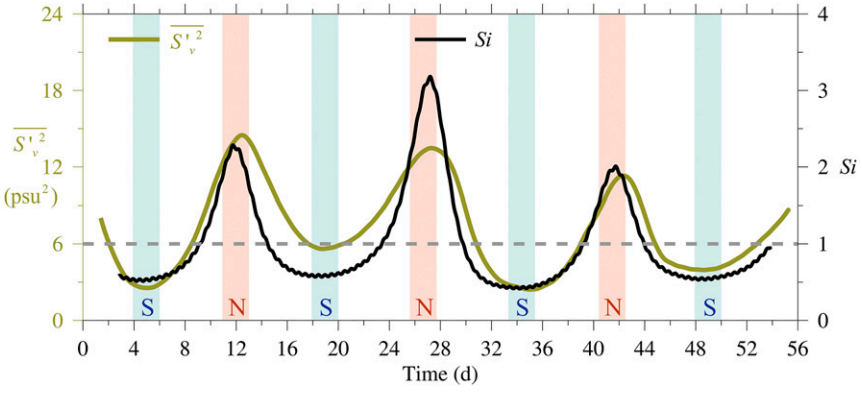

FIG. 12. Time series of volume averaged as well as low-pass filtered stratification (olive green) and Simpson number (black) in the estuarine domain V. The critical value of Si = 1 is represented by a gray dashed line.

because of the combination of strong shears and strong stratification. As expected the spring–neap cycle of tidal amplitude was found to strongly influence stratification but not expected was the large spring–neap variation in straining, with relatively less variation in dissipation of stratification.

The spatial and temporal variations of the terms in the vertical variance equation for the Changjiang estuary are informative in their own right, but such analysis gains more relevance when different systems are compared. For example, the analysis by Wang et al. (2017) of the variance balance in the Hudson estuary shows much greater variation of variance dissipation over the spring–neap cycle than exhibited by the Changjiang, even though stratification variations are comparable. How these quantities vary in more strongly and weakly stratified estuaries is yet to be determined, and such analysis is likely to provide valuable insights into the mechanisms responsible for transitions between well-mixed and stratified regimes.

Acknowledgments. X. Li was supported by the China Scholarship Council. W. R. Geyer was supported by NSF Grants OCE 1736539 and OCE 1634480. J. Zhu was supported by the National Natural Science Foundation of China (41476077 and 41676083). H. Wu was supported by the National Natural Science Foundation of China (41576088 and 41776101).

REFERENCES

Armi, L., and D. Farmer, 1986: Maximal two-layer exchange through a contraction with barotropic net flow. *J. Fluid Mech.*, **164**, 27–51, https://doi.org/10.1017/S0022112086002458.

Bowden, K. F., 1981: Turbulent mixing in estuaries. *Ocean Manage.*, **6**, 117–135, https://doi.org/10.1016/0302-184X(81)90033-0.

Bowen, M. M., and W. R. Geyer, 2003: Salt transport and the time-dependent salt balance of a partially stratified estuary. *J. Geophys. Res.*, **108**, 3158, https://doi.org/10.1029/2001JC001231.

Burchard, H., 2001: On the q^2l equation by Mellor and Yamada (1982). *J. Phys. Oceanogr.*, **31**, 1377–1387, https://doi.org/10.1175/1520-0485(2001)031<1377:OTQLEB>2.0.CO;2.

——, and H. Rennau, 2008: Comparative quantification of physically and numerically induced mixing in ocean models. *Ocean Modell.*, **20**, 293–311, https://doi.org/10.1016/j.ocemod.2007.10.003.

——, and H. M. Schuttelaars, 2012: Analysis of tidal straining as driver for estuarine circulation in well-mixed estuaries. *J. Phys. Oceanogr.*, **42**, 261–271, https://doi.org/10.1175/JPO-D-11-0110.1.

——, F. Janssen, K. Bolding, L. Umlauf, and H. Rennau, 2009: Model simulations of dense bottom currents in the western Baltic Sea. *Cont. Shelf Res.*, **29**, 205–220, https://doi.org/10.1016/j.csr.2007.09.010.

Cameron, W. M., and D. W. Pritchard, 1963: Estuaries. *The Composition of Sea-Water and Comparative and Descriptive Oceanography*, M. N. Hill, Ed., Vol. 2, *The Sea: Ideas and Observations on Progress in the Study of the Seas*, John Wiley and Sons, 306–324.

Galperin, B., L. Kantha, S. Hassid, and A. Rosati, 1988: A quasi-equilibrium turbulent energy model for geophysical flows. *J. Atmos. Sci.*, **45**, 55–62, https://doi.org/10.1175/1520-0469(1988)045<0055:AQETEM>2.0.CO;2.

Geyer, W. R., 1993: The importance of suppression of turbulence by stratification on the estuarine turbidity maximum. *Estuaries*, **16**, 113–125, https://doi.org/10.2307/1352769.

——, and P. MacCready, 2014: The estuarine circulation. *Annu. Rev. Fluid Mech.*, **46**, 175–197, https://doi.org/10.1146/annurev-fluid-010313-141302.

——, and D. K. Ralston, 2015: Estuarine frontogenesis. *J. Phys. Oceanogr.*, **45**, 546–561, https://doi.org/10.1175/JPO-D-14-0082.1.

——, R. C. Beardsley, S. J. Lentz, J. Candela, R. Limeburner, W. E. Johns, B. M. Castro, and I. D. Soares, 1996: Physical oceanography of the Amazon shelf. *Cont. Shelf Res.*, **16**, 575–616, https://doi.org/10.1016/0278-4343(95)00051-8.

Haas, L. W., 1977: The effect of the spring-neap tidal cycle on the vertical salinity structure of the James, York and Rappahannock Rivers, Virginia, U.S.A. *Estuarine Coastal Mar. Sci.*, **5**, 485–496, https://doi.org/10.1016/0302-3524(77)90096-2.

Hansen, D. V., and M. Rattray, 1965: Gravitational circulation in straits and estuaries. *J. Mar. Res.*, **23**, 104–122.

——, and ——, 1966: New dimensions in estuary classification. *Limnol. Oceanogr.*, **11**, 319–326, https://doi.org/10.4319/lo.1966.11.3.0319.

Horner-Devine, A. R., R. D. Hetland, and D. G. MacDonald, 2015: Mixing and transport in coastal river plumes. *Annu. Rev. Fluid Mech.*, **47**, 569–594, https://doi.org/10.1146/annurev-fluid-010313-141408.

Jay, D. A., and J. D. Smith, 1990: Circulation, density distribution and neap-spring transitions in the Columbia River estuary. *Prog. Oceanogr.*, **25**, 81–112, https://doi.org/10.1016/0079-6611(90)90004-L.

Lerczak, J. A., W. R. Geyer, and R. J. Chant, 2006: Mechanisms driving the time-dependent salt flux in a partially stratified estuary. *J. Phys. Oceanogr.*, **36**, 2296–2311, https://doi.org/10.1175/JPO2959.1.

Li, L., J. Zhu, H. Wu, and Z. Guo, 2014: Lateral saltwater intrusion in the North Channel of the Changjiang estuary. *Estuaries Coasts*, **37**, 36–55, https://doi.org/10.1007/s12237-013-9669-1.

Luketina, D. A., and J. Imberger, 1987: Characteristics of a surface buoyant jet. *J. Geophys. Res.*, **92**, 5435–5447, https://doi.org/10.1029/JC092iC05p05435.

Mellor, G. L., and T. Yamada, 1982: Development of a turbulence closure model for geophysical fluid problems. *Rev. Geophys.*, **20**, 851–875, https://doi.org/10.1029/RG020i004p00851.

Moon, J.-H., N. Hirose, J.-H. Yoon, and I.-C. Pang, 2010: Offshore detachment process of the low-salinity water around Changjiang Bank in the East China Sea. *J. Phys. Oceanogr.*, **40**, 1035–1053, https://doi.org/10.1175/2010JPO4167.1.

Nepf, H. M., and W. R. Geyer, 1996: Intratidal variations in stratification and mixing in the Hudson estuary. *J. Geophys. Res.*, **101**, 12 079–12 086, https://doi.org/10.1029/96JC00630.

Nunes Vaz, R. A., G. W. Lennon, and J. R. de Silva Samarasinghe, 1989: The negative role of turbulence in estuarine mass transport. *Estuarine Coastal Shelf Sci.*, **28**, 361–377, https://doi.org/10.1016/0272-7714(89)90085-1.

Peters, H., 1997: Observations of stratified turbulent mixing in an estuary: Neap-to-spring variations during high river flow. *Estuarine Coastal Shelf Sci.*, **45**, 69–88, https://doi.org/10.1006/ecss.1996.0180.

——, and R. Bokhorst, 2000: Microstructure observations of turbulent mixing in a partially mixed estuary. Part I: Dissipation rate. *J. Phys. Oceanogr.*, **30**, 1232–1244, https://doi.org/10.1175/1520-0485(2000)030<1232:MOOTMI>2.0.CO;2.

Qiu, C., and J. Zhu, 2013: Influence of seasonal runoff regulation by the Three Gorges Reservoir on saltwater intrusion in the Changjiang River estuary. *Cont. Shelf Res.*, **71**, 16–26, https://doi.org/10.1016/j.csr.2013.09.024.

Rennau, H., 2011: Natural, numerical and structure-induced mixing in dense gravity currents: Idealised and realistic model studies. Ph.D. dissertation, University of Rostock, 140 pp.

Simpson, J. H., J. Brown, J. Matthews, and G. Allen, 1990: Tidal straining, density currents, and stirring in the control of estuarine stratification. *Estuaries*, **13**, 125–132, https://doi.org/10.2307/1351581.

Stern, M. E., 1968: *T–S* gradients on the micro-scale. *Deep-Sea Res. Oceanogr. Abstr.*, **15**, 245–250, https://doi.org/10.1016/0011-7471(68)90001-6.

Sutherland, D. A., P. MacCready, N. S. Banas, and L. F. Smedstad, 2011: A model study of the Salish Sea estuarine circulation. *J. Phys. Oceanogr.*, **41**, 1125–1143, https://doi.org/10.1175/2011JPO4540.1.

Tennekes, H., and J. L. Lumley, 1972: *A First Course in Turbulence.* MIT Press, 300 pp.

Wang, T., W. R. Geyer, and P. MacCready, 2017: Total exchange flow, entrainment, and diffusive salt flux in estuaries. *J. Phys. Oceanogr.*, **47**, 1205–1220, https://doi.org/10.1175/JPO-D-16-0258.1.

Warner, J. C., C. R. Sherwood, H. G. Arango, and R. P. Signell, 2005: Performance of four turbulence closure models implemented using a generic length scale method. *Ocean Modell.*, **8**, 81–113, https://doi.org/10.1016/j.ocemod.2003.12.003.

Wu, H., and J. Zhu, 2010: Advection scheme with 3rd high-order spatial interpolation at the middle temporal level and its application to saltwater intrusion in the Changjiang estuary. *Ocean Modell.*, **33**, 33–51, https://doi.org/10.1016/j.ocemod.2009.12.001.

——, ——, J. Shen, and H. Wang, 2011: Tidal modulation on the Changjiang River plume in summer. *J. Geophys. Res.*, **116**, C08017, https://doi.org/10.1029/2011JC007209.

——, J. Shen, J. Zhu, J. Zhang, and L. Li, 2014: Characteristics of the Changjiang plume and its extension along the Jiangsu coast. *Cont. Shelf Res.*, **76**, 108–123, https://doi.org/10.1016/j.csr.2014.01.007.

Yankovsky, A. E., and D. C. Chapman, 1997: A simple theory for the fate of buoyant coastal discharges. *J. Phys. Oceanogr.*, **27**, 1386–1401, https://doi.org/10.1175/1520-0485(1997)027<1386:ASTFTF>2.0.CO;2.